J. Earth Planet. Sci. Nagoya Univ., Vol. 43, 49 to 65, 1996

# A preliminary CHIME age determination of monazites from metamorphic and granitic rocks in the Gyeonggi Massif, Korea

**Deung-Lyong CHO*, Kazuhiro SUZUKI**, Mamoru ADACHI** and Ueechan CHWAE***

**Geology Division, Korea Institute of Geology, Mining and Materials, 30 Kajeong-Dong, Yuseong-Ku, Daejeon, 305-350, Korea*
***Department of Earth and Planetary Sciences, Graduate School of Science, Nagoya University, Nagoya 461-01, Japan*
(Received November 1, 1996 / Accepted November 29, 1996)

## ABSTRACT

The CHIME (Chemical Th-U-Total Pb isochron method) dating was carried out for monazites from kyanite-staurolite-garnet schist of the Yeoncheon Group (Cheolwon area), and from sillimanite-garnet gneiss and two-mica granite in the central Gyeonggi Gneiss Complex (Hwacheon area). Monazites from the kyanite-staurolite-garnet schist yield an age of 255±8 Ma, and date the time of the regional metamorphism for the early-middle Proterozoic (?) Yeoncheon Group. Although the Gyeonggi Gneiss Complex has been believed to be of Archean–early Proterozoic age, monazites from the sillimanite-garnet gneiss yield a CHIME age of 245±3 Ma. Since one monazite grain from the gneiss contains ca. 1700 Ma core of detrital origin, the sedimentation of the gneiss protolith took place in the post-middle Proterozoic. The two-mica granite, intruding the Gyeonggi Gneiss Complex, yields a CHIME monazite age of 172±5 Ma. The present CHIME geochronological study reveals that metamorphic rocks not only in the Yeoncheon Group but also in some part of the Gyeonggi Gneiss Complex were formed through the ca. 250 Ma regional metamorphism. The late Permian–early Triassic metamorphism and Jurassic plutonism were more widespread than has been thought in the Korean Peninsula.

## INTRODUCTION

The Gyeonggi Massif occupies the central part of the Korean Peninsula, and together with the Yeongnam and Nangrim Massifs, it is one of the major tectonic units where metamorphic rocks widely occur (Fig. 1). Metamorphic rocks in the Gyeonggi Massif are divided into the Gyeonggi Gneiss Complex (Archean–early Proterozoic?) and the Yeoncheon and Seosan Groups (early to middle Proterozoic?). The former consists mainly of high-grade gneiss and schist, while the latter consists dominantly of low-grade schist, phyllite and slate (Na and Kim, 1987).

Three stages of metamorphism have been proposed within the Gyeonggi Massif: (1) Precambrian regional metamorphism of amphibolite facies, (2) post-Precambrian regional metamorphism, and (3) Jurassic thermal event

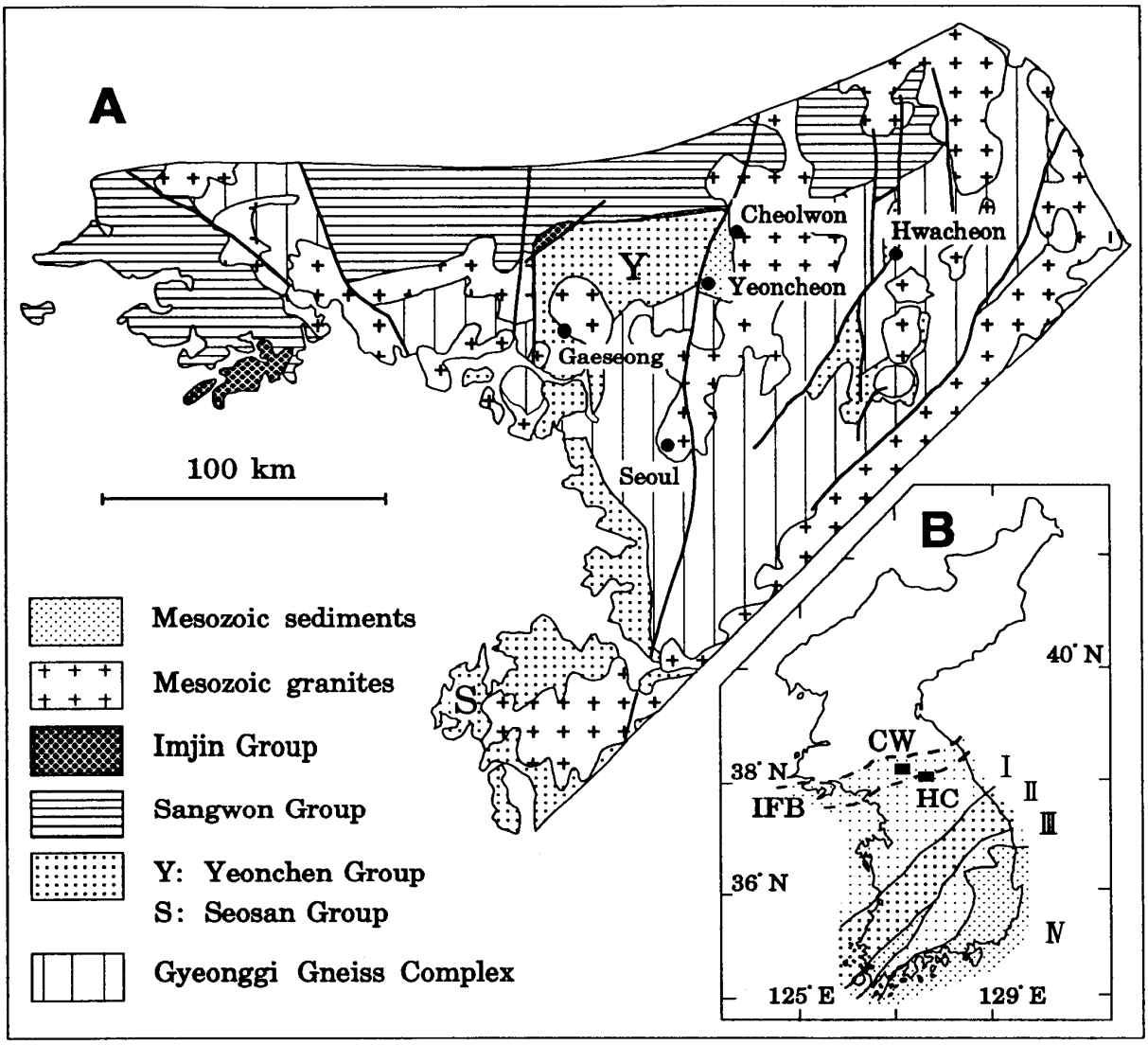


Fig. 1. Geologic framework of the Gyeonggi Massif, and location of the Cheolwon (CW) and Hwacheon (HC) areas. I: Gyeonggi Massif, II: Ogcheon Belt, III: Yeongnam Massif, IV: Gyeongsang Basin and IFB: Imjingang Fold Belt proposed by Ri and Ri (1990) and Cho et al. (1995). The Nangrim Massif distributed in the northern part of the insert map (B) is not shown.

possibly related to the intrusion of the Daebo Granites (Na, 1978). Systematic geochronological studies, however, have not been fully done in this massif, and reported K-Ar, Rb-Sr and Sm-Nd age data are widely scattered from late Proterozoic to middle Jurassic (Na and Lee, 1973; Lee et al., 1974; Na, 1977; Cho et al., 1995; Chwae et al., 1996).

In the northern part of the Gyeonggi Massif, there lies the so-called Imjingang Fold Belt (IFB in Fig. 1). This belt was originally named by North Korean geologists (Ri and Ri, 1990). The western part of the Imjingang Fold Belt is characterized by an EW structural trend, and comprises the Devonian volcano-sedimentary strata of the Imjin Group and some parts of the Gyeonggi Massif including the Yeoncheon Group (Chwae et al., 1996). Recently several

authors suggested that the Imjingang Fold Belt runs through the central part of the Korean Peninsula (Fig. 1), and together with the Ogcheon Fold Belt, it might be an eastward continuation of the Dabie-Sulu Collisional Belt in China (Ri and Ri, 1990; Cluzel et al., 1991; Cluzel, 1992, Liu, 1993; Yin and Nie, 1993; Ernst et al., 1994; Cho et al., 1995). However, northern and southern boundaries as well as westward and eastward continuations of the Imjingang Fold Belt have not been clearly defined yet. Furthermore, no ultra-high pressure indicator like diamond- or coesite-bearing eclogite in the Dabie-Sulu Belt has been known from the Imjingang Fold Belt.

To understand the tectonic evolution of the Gyeonggi Massif, we made a preliminary CHIME age determination on monazites from metamorphic rocks of the Yeoncheon Group and the Gyeonggi Gneiss Complex, and a granite intruding the Gyeonggi Gneiss Complex. This is the first CHIME age dating for the Gyeonggi Massif in the Korean Peninsula.

## GEOLOGICAL OUTLINE AND SAMPLE DESCRIPTION

Samples were collected from the Yeoncheon Group in the Cheolwon area and the Gyeonggi Gneiss Complex in the Hwacheon area (Fig. 1). These areas have been mapped in 1:50,000 scale under the national basic project of Korea Institute of Geology, Mining and Materials (KIGAM) (Chwae et al., 1996; Park et al., 1997).

### Cheolwon area

The geologic map of the Cheolwon area is given in Fig. 2. Metamorphosed strata in this area have been regarded as the Devonian Imjin Group. However, recently Chwae et al. (1996) reported that metamorphosed strata belong to the Yeoncheon Group, and newly divided them into the Misan, Daegwangri and Cheonduksan Formations in ascending order (Fig. 2). The Yeoncheon Group shows a general EW trend with dips toward north, and a reverse shear sense with 340° mineral stretching. Two different types of metamorphic rocks are identified in the Yeoncheon Group; one is low-grade metapsammite, phyllite and crystalline limestone, and the other includes amphibolite-facies pelitic schist of the garnet and kyanite zones of Barrovian type (Cho et al., 1995; Chwae et al., 1996).

One sample of medium-grained kyanite-staurolite-garnet schist (sample CH-10) from the Daegwangri Formation was selected for CHIME age dating (Fig. 2). It consists of quartz, plagioclase, biotite (partly chloritized), muscovite, garnet, staurolite, calcite and kyanite, with accessories of monazite, apatite and rutile. Monazite, tiny, less than 0.05 mm and anhedral, rarely occurs in biotite flakes.

### Hwacheon area

The Hwacheon area is about 60 km east of the Cheolwon area (Fig 1). As shown in Fig. 3, this area is underlain by metamorphic rocks and granitoids.

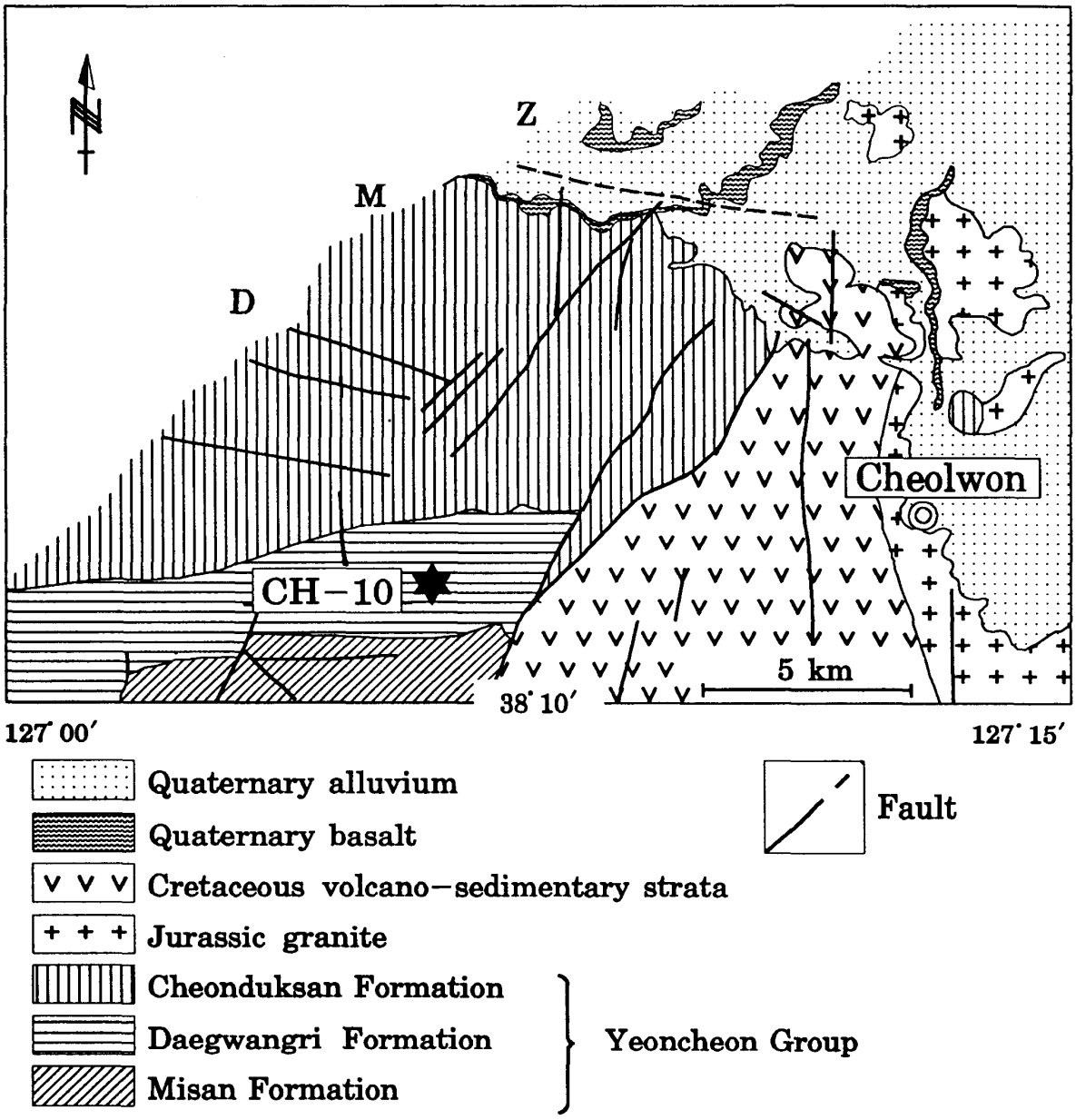


Fig. 2. Geologic map of the Cheolwon area and sample location (simplified and modified from Chwae et al., 1996). The Misan, Daegwangri and Cheonduksan Formations are included in the Middle Proterozoic (?) Yeoncheon Group. DMZ: demilitalized zone.

Several authors suggested that the northern part of the Hwacheon area belongs to the Imjingang Fold Belt (Fig. 1), and has undergone the granulite facies metamorphism (Ri and Ri, 1964; Lee and Cho, 1994; Cho et al., 1995).

Detailed mapping of the Hwacheon area (Park et al., 1997) revealed that amphibolite-facies metasedimentary rocks such as banded gneiss, migmatitic gneiss, biotite gneiss and mica schist are widely exposed, with subordinate garnet-bearing granite gneiss and amphibolite. The metasedimentary rocks of the Gyeonggi Gneiss Complex show well-developed gneissosity or schistosity. These planar structures show major trends of NE and NS. The EW

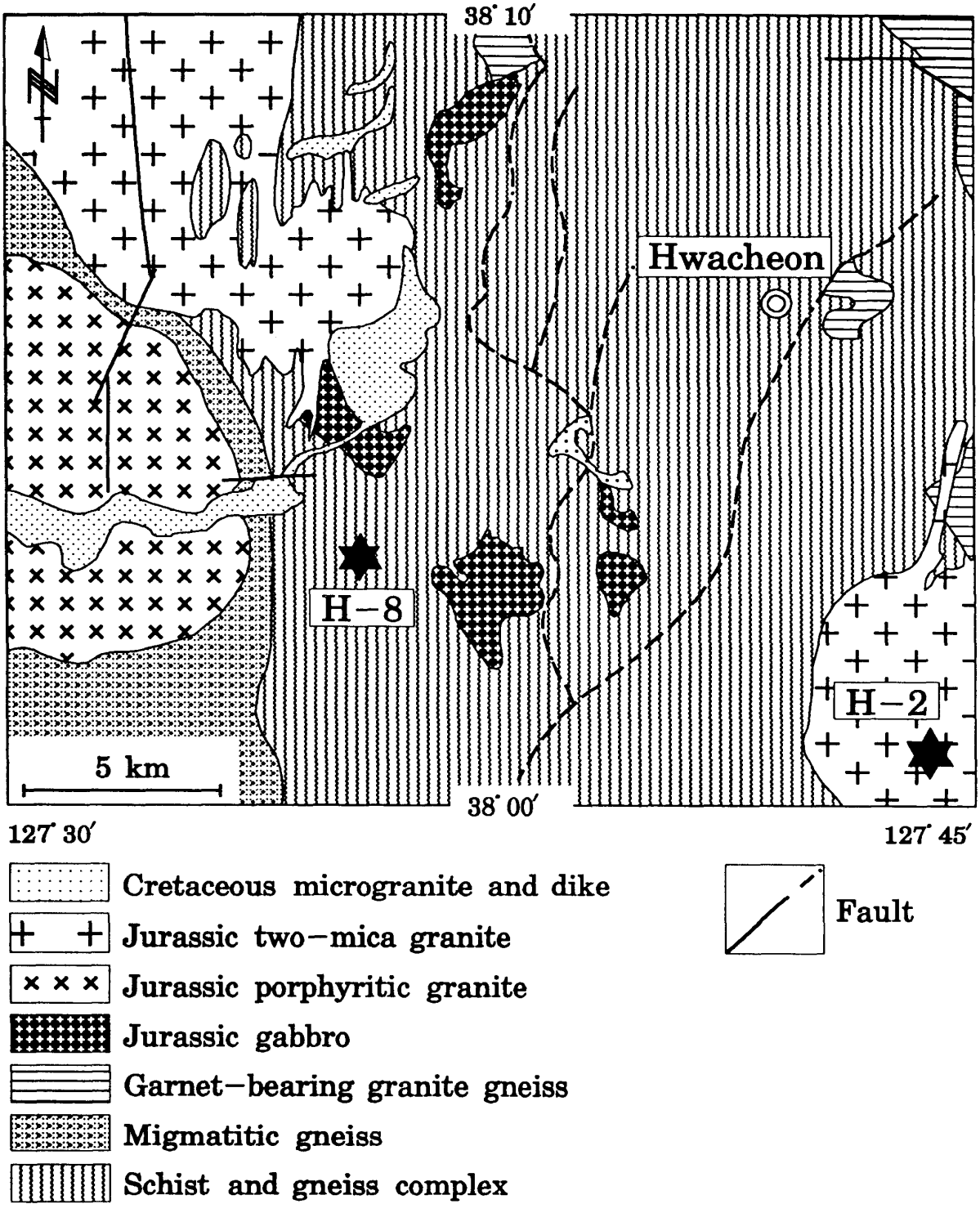


Fig. 3. Geologic map of the Hwacheon area and sample locations (simplified and modified from Park et al., 1997). The schist and gneiss complex, migmatitc gneiss and garnet-bearing granite gneiss are included in the Archean−early Proterozoic (?) Gyeonggi Gneiss Complex.

structural trend, dominant in the Cheolwon area, does not continue to the Hwacheon area.

Two samples were chosen for CHIME age dating (Fig. 3). They are sillimanite-garnet gneiss of the Gyeonggi Gneiss Complex and two-mica granite intruding the Gneiss Complex. The sillimanite-garnet gneiss (sample H-8) is medium-grained and consists of quartz, plagioclase, orthoclase, sillimanite, garnet, biotite and muscovite, with accessories of monazite, zircon (round), apatite and rutile. Small monazite grains are commonly found in biotite flakes. They are mostly 0.07—0.1 mm and subhedral, but larger (up to 0.2 mm) anhedral grains also occur rarely.

The two-mica granite (sample H-2) is massive and medium-grained, consisting mainly of quartz, plagioclase, perthitic microcline, biotite, muscovite and garnet. Accessory minerals include monazite and zircon. Hydrothermal or deuteric alteration of the granite is indicated by ubiquitous occurrence of sericite in plagioclase and chloritized biotite. Monazite grains, 0.03—0.1 mm, are subhedral or euhedral.

## SAMPLE PREPARATION AND ANALYSIS

Monazites in polished thin sections and/or mounted on glass slides with petropoxy were analyzed by using the JEOL JCXA-733 electron microprobe. Since details on procedures of sample preparation, microprobe analysis and CHIME age calculation were described elsewhere (Suzuki and Adachi, 1991a,b, 1994; Suzuki et al., 1991, 1994), we do not repeat them here. The $ThO_2$, $UO_2$ and PbO analyses of monazites, apparent ages and calculated $ThO_2$* concentrations are listed in Table 1.

## RESULTS

### Kyanite-staurolite-garnet schist (sample CH-10) from the Daegwangri Formation of the Yeoncheon Group

A total of 29 spots on 6 monazite grains were analyzed in polished thin sections. One monazite grain (M03) is extraordinarily rich in $ThO_2$ (23.0—28.2%) and $UO_2$ (1.54—2.14%), and is highly metamict. Spot M01-6, containing 19.8% $ThO_2$ and 1.31% $UO_2$, is also metamict. Except these data (cross in Fig. 4), the rest 24 data (circle in Fig. 4) show 3.50—12.5% of $ThO_2$, 0.10—0.65% of $UO_2$ and 0.044—0.140% of PbO. They are regressed by an isochron of $255 \pm 8$ Ma (MSWD = 0.10) with an intercept value of $-0.0011 \pm 0.0025$ (errors quoted in this paper for ages and intercept values are of $2\sigma$).

### Sillimanite-garnet gneiss (sample H-8) from the Gyeonggi Gneiss Complex

A total of 172 spots on 21 monazite grains were analyzed. Apparent ages of the most grains concentrate between 235 Ma and 258 Ma, and 118 data points (circle in Fig. 5) yield an isochron age of $245 \pm 3$ Ma (MSWD = 0.05) with an intercept value of $-0.0001 \pm 0.0011$ in the PbO vs. $ThO_2$* plot. The core part of

Table 1. Electron microprobe analyses of $ThO_2$, $UO_2$ and PbO of monazite grains from kyanite-staurolite-garnet schist of the Yeoncheon Group and sillimanite-garnet gneiss and two-mica granite in the Gyeonggi Gneiss Complex, Korea.

| Spot# | $ThO_2$ (wt.%) | $UO_2$ (wt.%) | PbO (wt.%) | Age (Ma) | $ThO_2$* (wt.%) |
|---|---|---|---|---|---|
| | Kyanite-staurolite-garnet schist (Sample CH-10) | | | | |
| M01-01 | 3.50 | 0.210 | 0.0440 | 249 | 4.18 |
| M01-02 | 4.23 | 0.451 | 0.0593 | 246 | 5.69 |
| M01-03 | 5.92 | 0.144 | 0.0716 | 265 | 6.39 |
| M01-04 | 8.26 | 0.160 | 0.0946 | 255 | 8.78 |
| M01-05 | 8.99 | 0.253 | 0.103 | 247 | 9.81 |
| M01-06 | 9.75 | 0.179 | 0.113 | 259 | 10.3 |
| M02-01 | 10.3 | 0.184 | 0.114 | 246 | 10.9 |
| M02-02 | 12.5 | 0.125 | 0.140 | 256 | 12.9 |
| M02-03 | 6.69 | 0.096 | 0.0715 | 241 | 7.01 |
| M02-04 | 6.87 | 0.132 | 0.0778 | 252 | 7.30 |
| M03-01m | 24.7 | 1.54 | 0.200 | 160 | 29.6 |
| M03-02m | 27.3 | 2.14 | 0.208 | 144 | 34.1 |
| M03-03m | 22.9 | 1.98 | 0.117 | 95 | 29.3 |
| M03-04m | 28.1 | 2.09 | 0.137 | 93 | 34.8 |
| M04-01 | 4.22 | 0.232 | 0.0526 | 250 | 4.97 |
| M04-02 | 7.09 | 0.328 | 0.0866 | 251 | 8.16 |
| M05-01 | 6.29 | 0.239 | 0.0725 | 243 | 7.06 |
| M05-02 | 5.26 | 0.216 | 0.0632 | 251 | 5.96 |
| M05-03 | 5.01 | 0.144 | 0.0578 | 249 | 5.48 |
| M05-04 | 4.43 | 0.255 | 0.0572 | 257 | 5.26 |
| M05-05 | 4.82 | 0.469 | 0.0676 | 252 | 6.34 |
| M05-06 | 7.75 | 0.451 | 0.0951 | 244 | 9.21 |
| M05-07 | 3.93 | 0.646 | 0.0680 | 267 | 6.02 |
| M05-08 | 4.24 | 0.288 | 0.0534 | 244 | 5.17 |
| M06-01m | 19.8 | 1.31 | 0.206 | 202 | 24.0 |
| M06-02 | 3.88 | 0.365 | 0.0530 | 247 | 5.07 |
| M06-03 | 4.41 | 0.435 | 0.0611 | 248 | 5.82 |
| M06-04 | 8.95 | 0.247 | 0.105 | 254 | 9.75 |
| M06-05 | 8.46 | 0.266 | 0.100 | 254 | 9.32 |

$ThO_2$*: sum of the measured $ThO_2$ and $ThO_2$ equivalent of the measured $UO_2$

Note;
- m: metamict part of monazite grain
- c: core part of monazite grain
- r: rim part of monazite grain
- s: sillimanite-containing monazite grain
- t: tiny monazite grain

| Spot# | $ThO_2$ (wt.%) | $UO_2$ (wt.%) | PbO (wt.%) | Age (Ma) | $ThO_2$* (wt.%) |
|---|---|---|---|---|---|
| | Sillimanite-garnet gneiss (Sample H-8) | | | | |
| M01-01 | 5.47 | 0.304 | 0.0662 | 242 | 6.46 |
| M01-02 | 5.71 | 0.297 | 0.0663 | 235 | 6.68 |
| M01-03 | 5.49 | 0.321 | 0.0688 | 249 | 6.53 |
| M01-04 | 5.15 | 0.376 | 0.0663 | 246 | 6.37 |
| M01-05 | 6.60 | 0.331 | 0.0778 | 240 | 7.67 |
| M01-06 | 3.76 | 0.353 | 0.0502 | 242 | 4.90 |
| M01-07 | 5.04 | 0.406 | 0.0658 | 244 | 6.36 |
| M01-08 | 6.00 | 0.415 | 0.0760 | 244 | 7.35 |
| M01-09 | 4.58 | 0.402 | 0.0643 | 258 | 5.89 |
| M01-10 | 6.10 | 0.376 | 0.0759 | 245 | 7.32 |
| M02-01 | 5.05 | 0.389 | 0.0665 | 249 | 6.31 |
| M02-02 | 5.97 | 0.340 | 0.0729 | 244 | 7.07 |
| M02-03 | 6.12 | 0.373 | 0.0760 | 245 | 7.33 |
| M02-04 | 5.97 | 0.363 | 0.0726 | 240 | 7.15 |
| M02-05 | 5.76 | 0.305 | 0.0701 | 246 | 6.75 |
| M02-06 | 5.52 | 0.348 | 0.0689 | 245 | 6.65 |
| M02-07 | 5.78 | 0.336 | 0.0716 | 246 | 6.86 |
| M02-08 | 5.08 | 0.289 | 0.0618 | 243 | 6.02 |
| M02-09 | 4.86 | 0.372 | 0.0632 | 246 | 6.06 |
| M02-10 | 5.46 | 0.393 | 0.0695 | 244 | 6.74 |
| M02-11 | 3.77 | 0.389 | 0.0521 | 245 | 5.03 |
| M02-12 | 5.84 | 0.294 | 0.0701 | 244 | 6.79 |
| M03-01s | 5.18 | 0.136 | 0.0441 | 186 | 5.62 |
| M03-02s | 5.37 | 0.176 | 0.0459 | 183 | 5.93 |
| M03-03s | 4.34 | 0.462 | 0.0588 | 238 | 5.84 |
| M03-04s | 5.10 | 0.150 | 0.0478 | 202 | 5.58 |
| M03-05s | 5.73 | 0.195 | 0.0495 | 184 | 6.36 |
| M04-01 | 8.73 | 0.354 | 0.101 | 243 | 9.87 |
| M04-02 | 10.3 | 0.398 | 0.120 | 244 | 11.6 |
| M04-03 | 6.81 | 0.417 | 0.0845 | 245 | 8.16 |
| M04-04 | 10.1 | 0.465 | 0.117 | 238 | 11.6 |
| M04-05 | 11.7 | 0.518 | 0.139 | 246 | 13.4 |
| M04-06 | 6.60 | 0.272 | 0.0770 | 243 | 7.48 |
| M05-01 | 5.87 | 0.320 | 0.0729 | 250 | 6.90 |
| M05-02 | 7.93 | 0.445 | 0.0958 | 241 | 9.38 |
| M05-03 | 5.64 | 0.458 | 0.0726 | 241 | 7.12 |
| M05-04 | 6.25 | 0.384 | 0.0782 | 246 | 7.50 |
| M05-05 | 6.03 | 0.336 | 0.0760 | 252 | 7.12 |
| M05-06 | 6.10 | 0.482 | 0.0782 | 241 | 7.67 |
| M05-07 | 5.43 | 0.510 | 0.0720 | 240 | 7.08 |
| M06-01 | 3.69 | 0.472 | 0.0531 | 240 | 5.22 |

Table 1. (continued).

| Spot# | $ThO_2$ (wt.%) | $UO_2$ (wt.%) | PbO (wt.%) | Age (Ma) | $ThO_2$* (wt.%) | Spot# | $ThO_2$ (wt.%) | $UO_2$ (wt.%) | PbO (wt.%) | Age (Ma) | $ThO_2$* (wt.%) |
|---|---|---|---|---|---|---|---|---|---|---|---|
| M06-02 | 3.12 | 0.491 | 0.0487 | 244 | 4.71 | M11-05 | 9.35 | 0.457 | 0.113 | 245 | 10.8 |
| M06-03 | 8.87 | 0.490 | 0.108 | 244 | 10.5 | M12-01t | 5.19 | 0.182 | 0.0502 | 205 | 5.78 |
| M06-04 | 6.61 | 0.403 | 0.0802 | 239 | 7.91 | M12-02t | 5.88 | 0.173 | 0.0495 | 182 | 6.44 |
| M07-01 | 6.93 | 0.484 | 0.0875 | 243 | 8.50 | M12-03t | 6.13 | 0.168 | 0.0564 | 200 | 6.67 |
| M07-02 | 11.2 | 0.404 | 0.129 | 242 | 12.5 | M12-04t | 6.11 | 0.173 | 0.0621 | 220 | 6.67 |
| M07-03 | 9.63 | 0.389 | 0.114 | 247 | 10.9 | M13-01 | 6.46 | 0.360 | 0.0786 | 244 | 7.62 |
| M08-01d | 5.62 | 0.382 | 0.511 | 1661 | 7.03 | M13-02 | 7.20 | 0.473 | 0.0890 | 241 | 8.74 |
| M08-02d | 5.56 | 0.392 | 0.518 | 1690 | 7.00 | M13-03r | 5.72 | 0.243 | 0.0492 | 179 | 6.51 |
| M08-03d | 5.54 | 0.415 | 0.520 | 1682 | 7.06 | M13-04 | 5.76 | 0.233 | 0.0673 | 244 | 6.51 |
| M08-04d | 5.65 | 0.399 | 0.531 | 1701 | 7.12 | M14-01 | 11.1 | 0.373 | 0.127 | 245 | 12.3 |
| M08-05d | 5.61 | 0.395 | 0.508 | 1644 | 7.06 | M14-02 | 11.2 | 0.348 | 0.129 | 246 | 12.3 |
| M08-06d | 5.58 | 0.407 | 0.523 | 1687 | 7.07 | M14-03 | 8.96 | 0.528 | 0.110 | 244 | 10.7 |
| M08-07d | 5.42 | 0.365 | 0.513 | 1730 | 6.77 | M14-04 | 10.1 | 0.377 | 0.119 | 249 | 11.3 |
| M08-08d | 5.33 | 0.366 | 0.508 | 1733 | 6.68 | M14-05 | 13.2 | 0.324 | 0.149 | 247 | 14.3 |
| M08-09d | 5.40 | 0.421 | 0.508 | 1670 | 6.95 | M15-01r | 5.68 | 0.151 | 0.0500 | 192 | 6.17 |
| M08-10d | 5.49 | 0.406 | 0.500 | 1637 | 6.98 | M15-02 | 5.57 | 0.157 | 0.0646 | 251 | 6.08 |
| M08-11r | 6.47 | 0.294 | 0.0626 | 199 | 7.42 | M15-03 | 5.90 | 0.165 | 0.0630 | 231 | 6.43 |
| M08-12 | 6.65 | 0.270 | 0.0753 | 237 | 7.52 | M15-04 | 5.62 | 0.150 | 0.0624 | 242 | 6.10 |
| M08-13 | 5.57 | 0.267 | 0.0633 | 232 | 6.44 | M16-01r | 5.33 | 0.397 | 0.0646 | 231 | 6.61 |
| M08-14 | 5.42 | 0.244 | 0.0644 | 245 | 6.21 | M16-02 | 5.26 | 0.362 | 0.0655 | 241 | 6.44 |
| M08-15 | 5.71 | 0.248 | 0.0591 | 215 | 6.51 | M16-03r | 5.67 | 0.363 | 0.0628 | 217 | 6.84 |
| M08-16d | 5.80 | 0.413 | 0.551 | 1717 | 7.32 | M16-04r | 6.64 | 0.450 | 0.0825 | 241 | 8.10 |
| M08-17d | 5.74 | 0.419 | 0.497 | 1567 | 7.26 | M16-05 | 6.21 | 0.501 | 0.0834 | 252 | 7.83 |
| M08-18 | 4.61 | 0.258 | 0.0560 | 243 | 5.44 | M16-06r | 6.59 | 0.461 | 0.0797 | 233 | 8.09 |
| M08-19 | 4.36 | 0.282 | 0.0569 | 255 | 5.28 | M16-07r | 4.99 | 0.422 | 0.0622 | 231 | 6.35 |
| M08-20d | 5.60 | 0.348 | 0.143 | 497 | 6.75 | M16-08 | 5.71 | 0.427 | 0.0739 | 246 | 7.09 |
| M08-21 | 6.34 | 0.331 | 0.0698 | 223 | 7.41 | M16-09 | 5.51 | 0.383 | 0.0696 | 244 | 6.75 |
| M08-22d | 5.91 | 0.344 | 0.533 | 1697 | 7.17 | M16-10 | 6.04 | 0.342 | 0.0745 | 246 | 7.15 |
| M08-23d | 5.54 | 0.328 | 0.510 | 1723 | 6.75 | M16-11 | 5.51 | 0.355 | 0.0714 | 253 | 6.66 |
| M08-24d | 7.12 | 0.379 | 0.197 | 552 | 8.38 | M16-12 | 5.30 | 0.343 | 0.0644 | 237 | 6.41 |
| M08-25d | 5.43 | 0.391 | 0.509 | 1691 | 6.87 | M16-13r | 4.38 | 0.388 | 0.0564 | 236 | 5.64 |
| M08-26d | 5.65 | 0.373 | 0.529 | 1718 | 7.03 | M16-14r | 5.93 | 0.397 | 0.0699 | 229 | 7.21 |
| M09-01 | 5.92 | 0.579 | 0.0842 | 255 | 7.79 | M16-15 | 6.31 | 0.400 | 0.0830 | 258 | 7.60 |
| M09-02 | 5.99 | 0.607 | 0.0841 | 250 | 7.95 | M16-16 | 5.86 | 0.353 | 0.0730 | 246 | 7.00 |
| M09-03 | 5.51 | 0.558 | 0.0750 | 242 | 7.32 | M16-17 | 5.66 | 0.362 | 0.0712 | 246 | 6.84 |
| M10-01 | 5.56 | 0.316 | 0.0699 | 251 | 6.59 | M16-18 | 5.60 | 0.341 | 0.0698 | 246 | 6.71 |
| M10-02r | 5.37 | 0.328 | 0.0516 | 190 | 6.43 | M16-19 | 5.31 | 0.324 | 0.0678 | 252 | 6.36 |
| M10-03r | 5.46 | 0.313 | 0.0584 | 213 | 6.47 | M16-20 | 5.62 | 0.353 | 0.0695 | 243 | 6.76 |
| M10-04 | 5.09 | 0.317 | 0.0616 | 238 | 6.12 | M16-21 | 4.42 | 0.276 | 0.0573 | 255 | 5.32 |
| M10-05 | 5.44 | 0.312 | 0.0663 | 243 | 6.45 | M16-22r | 5.99 | 0.359 | 0.0714 | 236 | 7.15 |
| M11-02 | 5.55 | 0.310 | 0.0695 | 250 | 6.56 | M16-23r | 5.61 | 0.294 | 0.0590 | 213 | 6.56 |
| M11-02 | 6.22 | 0.441 | 0.0799 | 247 | 7.64 | M16-24 | 5.39 | 0.312 | 0.0650 | 240 | 6.40 |
| M11-03 | 6.87 | 0.379 | 0.0839 | 245 | 8.10 | M16-25 | 5.73 | 0.269 | 0.0681 | 244 | 6.60 |
| M11-04 | 6.59 | 0.314 | 0.0791 | 246 | 7.60 | M16-26 | 5.44 | 0.290 | 0.0671 | 248 | 6.39 |

Table 1. (continued).

| Spot# | $ThO_2$ (wt.%) | $UO_2$ (wt.%) | PbO (wt.%) | Age (Ma) | $ThO_2$* (wt.%) |
|---|---|---|---|---|---|
| M16-27 | 4.91 | 0.275 | 0.0600 | 245 | 5.80 |
| M16-28 | 5.86 | 0.340 | 0.0709 | 241 | 6.96 |
| M16-29r | 6.34 | 0.308 | 0.0695 | 224 | 7.33 |
| M16-30r | 5.24 | 0.335 | 0.0601 | 225 | 6.32 |
| M16-31 | 6.18 | 0.460 | 0.0778 | 240 | 7.67 |
| M16-32 | 5.00 | 0.329 | 0.0630 | 245 | 6.06 |
| M16-33 | 5.88 | 0.332 | 0.0725 | 246 | 6.95 |
| M16-34 | 5.56 | 0.323 | 0.0683 | 244 | 6.61 |
| M16-35 | 5.57 | 0.264 | 0.0669 | 246 | 6.42 |
| M16-36 | 6.06 | 0.289 | 0.0713 | 241 | 7.00 |
| M16-37 | 6.06 | 0.307 | 0.0716 | 240 | 7.05 |
| M16-38r | 5.95 | 0.302 | 0.0697 | 238 | 6.93 |
| M17-01 | 5.17 | 0.271 | 0.0620 | 242 | 6.05 |
| M17-02 | 5.43 | 0.292 | 0.0648 | 240 | 6.38 |
| M17-03 | 5.35 | 0.306 | 0.0661 | 246 | 6.34 |
| M17-04 | 5.65 | 0.252 | 0.0642 | 235 | 6.46 |
| M17-05 | 5.34 | 0.276 | 0.0639 | 242 | 6.23 |
| M18-01 | 4.69 | 0.266 | 0.0602 | 256 | 5.55 |
| M18-02 | 5.37 | 0.285 | 0.0642 | 241 | 6.29 |
| M18-03 | 4.71 | 0.270 | 0.0596 | 252 | 5.59 |
| M18-04 | 4.65 | 0.384 | 0.0585 | 235 | 5.89 |
| M18-05 | 5.92 | 0.373 | 0.0749 | 248 | 7.13 |
| M19-01r | 4.89 | 0.266 | 0.0497 | 205 | 5.74 |
| M19-02 | 5.11 | 0.279 | 0.0616 | 242 | 6.02 |
| M19-03 | 5.12 | 0.289 | 0.0606 | 236 | 6.06 |
| M19-04r | 3.92 | 0.539 | 0.0519 | 217 | 5.66 |
| M19-05 | 5.31 | 0.329 | 0.0659 | 244 | 6.38 |
| M20-01 | 7.09 | 0.305 | 0.0825 | 241 | 8.08 |
| M20-02 | 5.47 | 0.330 | 0.0682 | 246 | 6.54 |
| M20-03 | 5.29 | 0.289 | 0.0659 | 250 | 6.22 |
| M20-04 | 5.68 | 0.336 | 0.0747 | 261 | 6.77 |
| M20-05 | 4.98 | 0.247 | 0.0574 | 235 | 5.78 |
| M20-06 | 4.98 | 0.250 | 0.0588 | 240 | 5.79 |
| M20-07 | 5.66 | 0.275 | 0.0696 | 251 | 6.55 |
| M20-08 | 4.55 | 0.269 | 0.0540 | 235 | 5.42 |
| M21-01 | 5.19 | 0.295 | 0.0626 | 241 | 6.15 |
| M21-02 | 5.11 | 0.304 | 0.0645 | 250 | 6.09 |
| M21-03 | 5.21 | 0.284 | 0.0633 | 244 | 6.13 |
| M21-04 | 5.13 | 0.294 | 0.0642 | 250 | 6.08 |
| M21-05 | 5.01 | 0.274 | 0.0633 | 253 | 5.90 |
| M21-06 | 5.46 | 0.305 | 0.0672 | 246 | 6.45 |
| M21-07 | 4.83 | 0.256 | 0.0580 | 242 | 5.66 |
| M21-08r | 4.96 | 0.247 | 0.0504 | 207 | 5.76 |

| Spot# | $ThO_2$ (wt.%) | $UO_2$ (wt.%) | PbO (wt.%) | Age (Ma) | $ThO_2$* (wt.%) |
|---|---|---|---|---|---|
| | Two-mica granite (Sample H-2) | | | | |
| M01-01 | 9.89 | 0.275 | 0.0780 | 171 | 10.8 |
| M01-02 | 10.6 | 0.206 | 0.0883 | 185 | 11.3 |
| M01-03 | 10.5 | 0.198 | 0.0806 | 171 | 11.2 |
| M01-04c | 5.99 | 0.146 | 0.0529 | 194 | 6.46 |
| M01-05 | 10.2 | 0.187 | 0.0848 | 186 | 10.8 |
| M01-06 | 8.51 | 0.202 | 0.0669 | 173 | 9.16 |
| M01-07c | 5.40 | 0.182 | 0.0539 | 213 | 5.99 |
| M01-08 | 10.4 | 0.186 | 0.0802 | 172 | 11.0 |
| M01-09 | 5.58 | 0.137 | 0.0415 | 163 | 6.03 |
| M02-01c | 5.26 | 0.132 | 0.0484 | 201 | 5.69 |
| M02-02 | 4.73 | 0.121 | 0.0380 | 175 | 5.12 |
| M02-03 | 13.5 | 0.214 | 0.107 | 178 | 14.2 |
| M02-04 | 14.0 | 0.248 | 0.112 | 179 | 14.8 |
| M02-05 | 12.8 | 0.198 | 0.101 | 178 | 13.4 |
| M02-06 | 13.1 | 0.200 | 0.0967 | 167 | 13.7 |
| M02-07 | 13.9 | 0.243 | 0.100 | 161 | 14.7 |
| M02-08 | 17.8 | 0.373 | 0.141 | 175 | 19.0 |
| M02-09 | 13.2 | 0.218 | 0.100 | 170 | 13.9 |
| M02-10 | 9.31 | 0.187 | 0.0776 | 185 | 9.91 |
| M02-11 | 12.3 | 0.209 | 0.0938 | 171 | 12.9 |
| M02-12c | 8.99 | 0.151 | 0.0818 | 204 | 9.48 |
| M02-13r | 6.13 | 0.309 | 0.0419 | 139 | 7.12 |
| M02-14 | 8.59 | 0.224 | 0.0629 | 160 | 9.31 |
| M02-15c | 8.83 | 0.161 | 0.0791 | 200 | 9.35 |
| M02-16c | 5.65 | 0.550 | 0.0639 | 203 | 7.43 |
| M03-01 | 9.53 | 0.084 | 0.0762 | 184 | 9.80 |
| M03-02 | 9.86 | 0.104 | 0.0760 | 176 | 10.2 |
| M03-03 | 10.2 | 0.150 | 0.0754 | 168 | 10.6 |
| M03-04 | 8.99 | 0.110 | 0.0641 | 162 | 9.34 |
| M03-05 | 9.86 | 0.109 | 0.0803 | 186 | 10.2 |
| M03-06 | 6.87 | 0.055 | 0.0508 | 170 | 7.05 |
| M03-07 | 6.91 | 0.036 | 0.0525 | 177 | 7.03 |
| M03-08c | 10.4 | 0.117 | 0.0935 | 205 | 10.8 |
| M03-09c | 10.2 | 0.097 | 0.0884 | 199 | 10.5 |
| M03-10 | 10.0 | 0.114 | 0.0809 | 185 | 10.4 |
| M03-11 | 10.0 | 0.100 | 0.0806 | 184 | 10.4 |
| M03-12 | 9.63 | 0.097 | 0.0695 | 165 | 9.94 |
| M03-13c | 10.3 | 0.099 | 0.0878 | 195 | 10.6 |
| M03-14 | 10.4 | 0.117 | 0.0783 | 173 | 10.7 |
| M03-16 | 10.1 | 0.095 | 0.0767 | 174 | 10.4 |
| M04-01 | 8.53 | 0.224 | 0.0716 | 183 | 9.25 |
| M04-02 | 4.03 | 0.083 | 0.0326 | 180 | 4.29 |

Table 1. (continued).

| Spot# | $ThO_2$ (wt.%) | $UO_2$ (wt.%) | PbO (wt.%) | Age (Ma) | $ThO_2$* (wt.%) | Spot# | $ThO_2$ (wt.%) | $UO_2$ (wt.%) | PbO (wt.%) | Age (Ma) | $ThO_2$* (wt.%) |
|---|---|---|---|---|---|---|---|---|---|---|---|
| M04-03 | 4.71 | 0.134 | 0.0415 | 191 | 5.15 | M05-42r | 2.42 | 0.179 | 0.0177 | 140 | 3.00 |
| M04-04c | 7.11 | 0.043 | 0.0605 | 197 | 7.25 | M05-43 | 3.71 | 0.094 | 0.0294 | 173 | 4.01 |
| M04-05 | 8.54 | 0.048 | 0.0661 | 180 | 8.69 | M05-44c | 3.43 | 0.116 | 0.0313 | 194 | 3.81 |
| M05-01 | 5.78 | 0.222 | 0.0472 | 172 | 6.49 | M04-45 | 3.39 | 0.112 | 0.0248 | 156 | 3.75 |
| M05-02r | 5.81 | 0.240 | 0.0268 | 96 | 6.58 | M05-46 | 3.16 | 0.070 | 0.0238 | 167 | 3.38 |
| M05-03 | 7.83 | 0.379 | 0.0609 | 159 | 9.06 | M05-47 | 3.59 | 0.091 | 0.0281 | 171 | 3.88 |
| M05-04 | 6.30 | 0.133 | 0.0523 | 184 | 6.73 | M05-48r | 6.24 | 0.060 | 0.0403 | 148 | 6.43 |
| M05-05r | 6.82 | 0.197 | 0.0236 | 75 | 7.45 | M05-49 | 4.96 | 0.119 | 0.0349 | 155 | 5.34 |
| M05-06r | 6.14 | 0.340 | 0.0353 | 116 | 7.23 | M05-50r | 4.25 | 0.115 | 0.0258 | 132 | 4.62 |
| M05-07 | 5.04 | 0.189 | 0.0454 | 190 | 5.65 | M05-51 | 3.58 | 0.120 | 0.0295 | 176 | 3.97 |
| M05-08 | 6.13 | 0.260 | 0.0569 | 193 | 6.97 | M05-52r | 1.96 | 0.314 | 0.0167 | 133 | 2.97 |
| M05-09r | 6.03 | 0.361 | 0.0224 | 74 | 7.19 | M05-53 | 3.20 | 0.122 | 0.0270 | 177 | 3.60 |
| M05-10r | 6.56 | 0.150 | 0.0386 | 130 | 7.04 | M05-54r | 2.64 | 0.211 | 0.0185 | 132 | 3.32 |
| M05-11 | 6.25 | 0.110 | 0.0453 | 162 | 6.60 | M05-55r | 2.76 | 0.124 | 0.0198 | 148 | 3.16 |
| M05-12 | 6.24 | 0.166 | 0.0453 | 158 | 6.77 | M05-56 | 3.24 | 0.185 | 0.0254 | 157 | 3.84 |
| M05-13 | 5.78 | 0.131 | 0.0425 | 162 | 6.20 | M05-57 | 3.37 | 0.103 | 0.0252 | 161 | 3.71 |
| M05-14r | 5.29 | 0.125 | 0.0316 | 131 | 5.69 | M05-58 | 3.88 | 0.104 | 0.0301 | 169 | 4.21 |
| M05-15 | 6.61 | 0.179 | 0.0481 | 158 | 7.18 | M05-59c | 3.73 | 0.105 | 0.0344 | 200 | 4.07 |
| M05-16r | 6.40 | 0.173 | 0.0435 | 148 | 6.96 | M05-60 | 2.84 | 0.106 | 0.0257 | 191 | 3.18 |
| M05-17 | 4.95 | 0.081 | 0.0409 | 186 | 5.21 | M05-61r | 3.60 | 0.250 | 0.0189 | 101 | 4.40 |
| M05-18c | 3.06 | 0.107 | 0.0332 | 231 | 3.40 | M05-62r | 2.89 | 0.199 | 0.0221 | 148 | 3.53 |
| M05-19r | 4.56 | 0.105 | 0.0249 | 120 | 4.90 | M05-63 | 2.19 | 0.154 | 0.0209 | 184 | 2.69 |
| M05-20 | 3.88 | 0.102 | 0.0326 | 183 | 4.20 | M05-64 | 1.72 | 0.191 | 0.0193 | 196 | 2.33 |
| M05-21 | 4.14 | 0.086 | 0.0288 | 154 | 4.41 | M05-65 | 1.79 | 0.306 | 0.0227 | 193 | 2.78 |
| M05-22r | 5.07 | 0.131 | 0.0340 | 147 | 5.49 | M05-66 | 2.71 | 0.174 | 0.0231 | 167 | 3.28 |
| M05-23 | 6.18 | 0.142 | 0.0447 | 159 | 6.64 | M05-67c | 3.58 | 0.176 | 0.0404 | 230 | 4.14 |
| M05-24r | 5.87 | 0.088 | 0.0382 | 147 | 6.15 | M05-68r | 3.40 | 0.128 | 0.0198 | 123 | 3.81 |
| M05-25 | 3.96 | 0.036 | 0.0272 | 158 | 4.08 | M05-69c | 5.19 | 0.055 | 0.0468 | 206 | 5.37 |
| M05-26c | 3.55 | 0.040 | 0.0378 | 243 | 3.68 | M05-70 | 3.83 | 0.118 | 0.0293 | 165 | 4.21 |
| M05-27r | 6.45 | 0.145 | 0.0437 | 150 | 6.91 | M05-71 | 3.22 | 0.116 | 0.0288 | 190 | 3.59 |
| M05-28r | 6.07 | 0.152 | 0.0382 | 138 | 6.56 | M05-72c | 3.28 | 0.112 | 0.0351 | 228 | 3.64 |
| M05-29 | 5.95 | 0.139 | 0.0459 | 170 | 6.40 | M05-73 | 3.98 | 0.047 | 0.0328 | 188 | 4.13 |
| M05-30r | 5.08 | 0.121 | 0.0356 | 154 | 5.47 | M05-74 | 3.07 | 0.002 | 0.0220 | 169 | 3.07 |
| M05-31r | 3.80 | 0.108 | 0.0252 | 144 | 4.14 | M05-75 | 4.34 | 0.065 | 0.0352 | 183 | 4.55 |
| M05-32 | 4.01 | 0.097 | 0.0327 | 179 | 4.32 | M05-76c | 3.79 | 0.096 | 0.0452 | 261 | 4.10 |
| M05-33 | 3.87 | 0.083 | 0.0285 | 163 | 4.14 | M05-77 | 4.56 | 0.122 | 0.0369 | 176 | 4.96 |
| M05-34 | 4.73 | 0.066 | 0.0391 | 187 | 4.94 | M05-78c | 4.81 | 0.109 | 0.0456 | 209 | 5.16 |
| M05-35 | 5.82 | 0.192 | 0.0429 | 158 | 6.44 | M05-79 | 3.53 | 0.071 | 0.0294 | 185 | 3.76 |
| M05-36 | 5.55 | 0.157 | 0.0433 | 169 | 6.06 | M05-80r | 4.98 | 0.109 | 0.0286 | 127 | 5.33 |
| M05-37r | 5.26 | 0.144 | 0.0359 | 148 | 5.72 | M05-81 | 3.90 | 0.328 | 0.0332 | 158 | 4.96 |
| M05-38 | 4.45 | 0.136 | 0.0451 | 218 | 4.89 | M05-82 | 3.30 | 0.265 | 0.0305 | 174 | 4.16 |
| M05-39c | 6.64 | 0.342 | 0.0662 | 202 | 7.74 | M05-83 | 6.60 | 0.184 | 0.0568 | 187 | 7.19 |
| M05-40c | 3.88 | 0.100 | 0.0365 | 205 | 4.20 | | | | | | |
| M05-41 | 3.69 | 0.080 | 0.0304 | 182 | 3.95 | | | | | | |

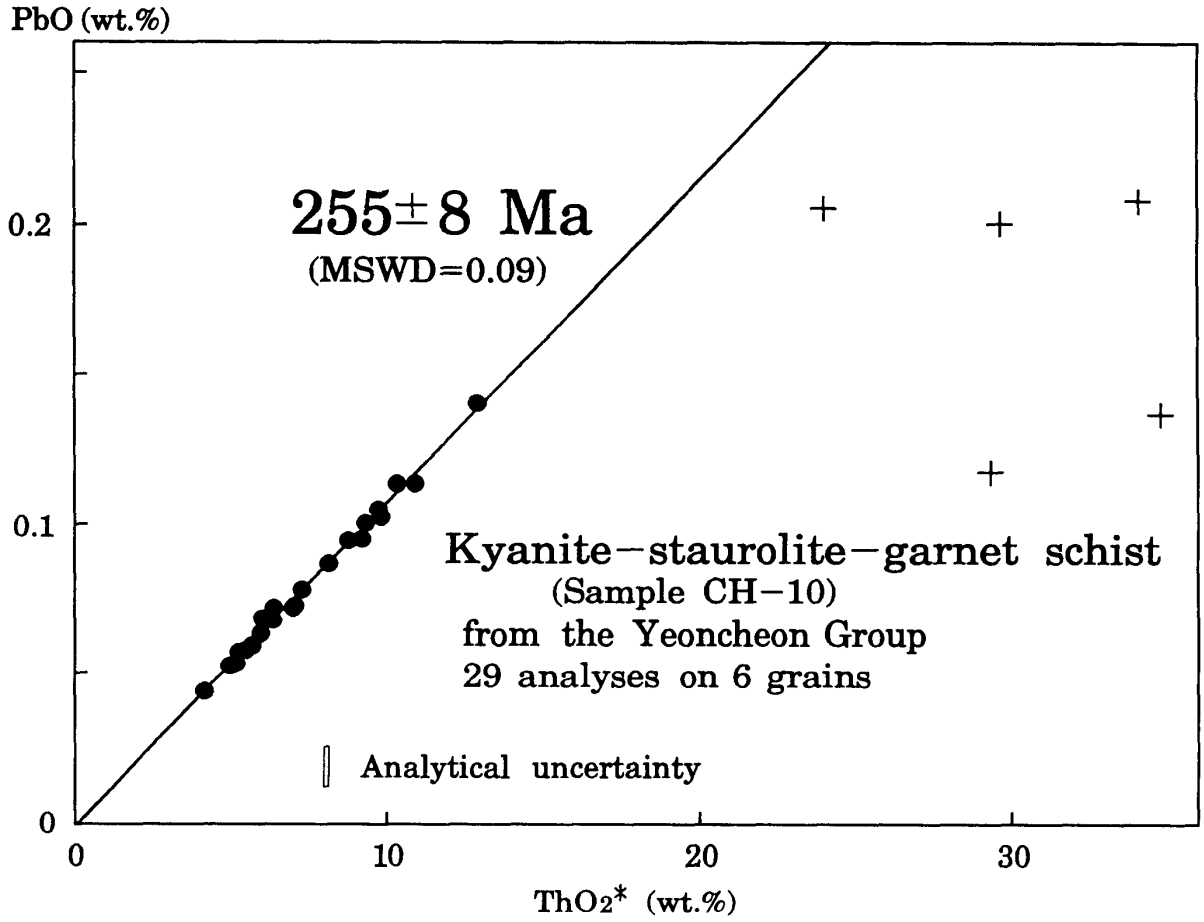


Fig. 4. Plots of PbO vs. $ThO_2$* of monazite grains from the kyanite-staurolite-garnet schist (sample CH-10) of the Yeoncheon Group. Circles represent data points for transparent portions, and crosses do data points for metamict portions. Error box in the figure represents $2\sigma$ analytical uncertainty, and error quoted for age is of $2\sigma$.

M8 grain (square in Fig. 5) is much older than others, concentrating around the 1700 Ma reference isochron. The core also differs in composition ($ThO_2/UO_2 = 12-17$) from the ca. 245 Ma rim ($ThO_2/UO_2 = 15-24$). The ca. 1700 Ma core, formed under different chemical environments from the ca. 245 Ma rim, appears to be detrital. One monazite grain (M03) contains sillimanite (fibrolite) in its rim portion, indicating an overgrowth after the formation of sillimanite. The core of M03 grain shows 238 Ma apparent age, while the sillimanite-containing rim gives 183−186 Ma apparent ages. Similar young ages (cross in Fig. 5) are also recognized from a tiny grain (M12) and rims of some large grains (M13 and M15). The age zoning of monazite suggests that the sillimanite-garnet gneiss underwent an intensive thermal event during Jurassic time after the ca. 245 Ma high-grade metamorphism.

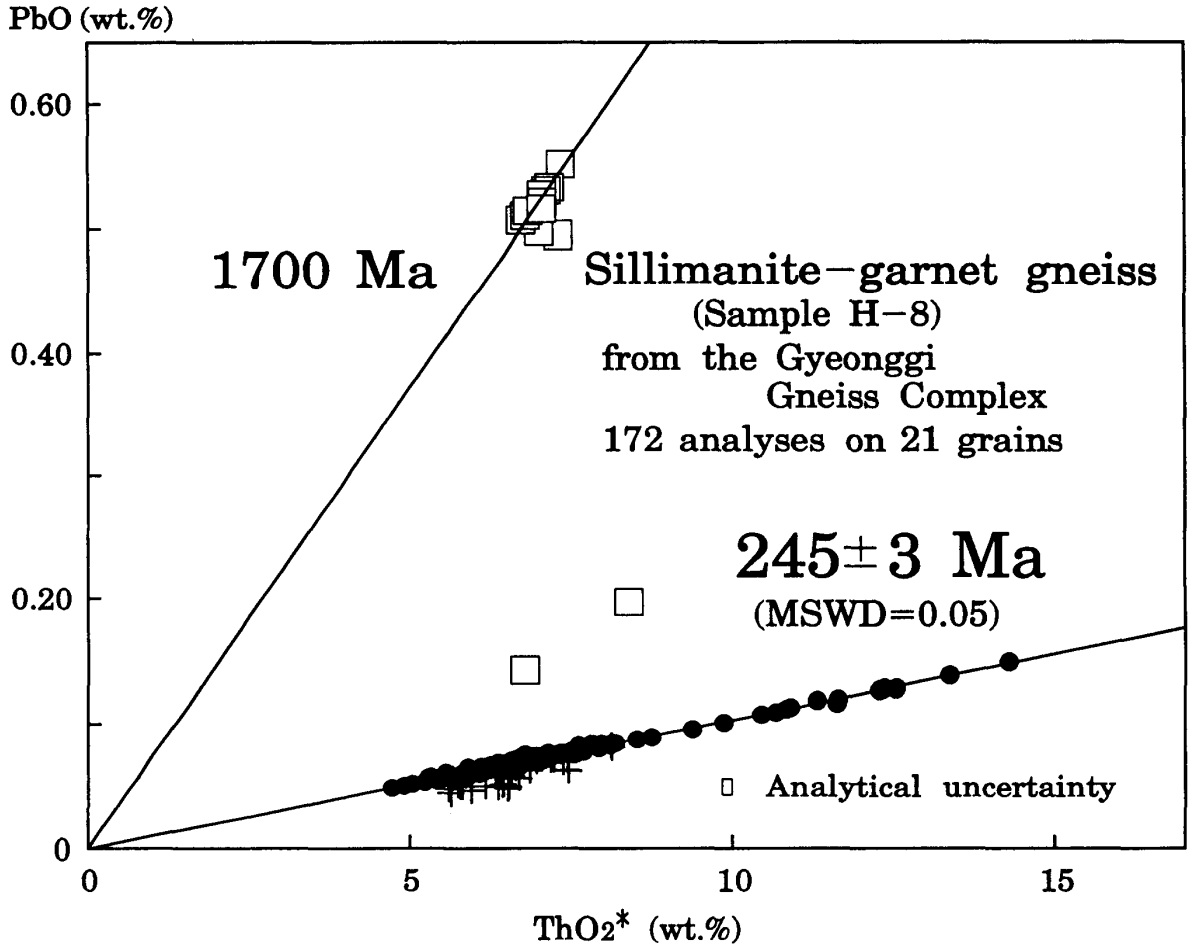


Fig. 5. Plots of PbO vs. $ThO_2$* of monazite grains from the sillimanite-garnet gneiss in the Gyeonggi Gneiss Complex (sample H-8). Circles represent data points used for age calculation. Data points for the core of zoned M08 grain are shown by squares, and those for sillimanite-containing M03 grain, tiny M12 grain and rim portions of unzoned grains are shown by crosses. Explanation for errors is the same as Fig. 3.

**Two-mica granite (sample H-2) from the Gyeonggi Gneiss Complex**

A total of 128 spots on 5 monazite grains were analyzed. Some spots on the cores of individual grains (square in Fig. 6) show apparent ages of 190–261 Ma, and those on grain edges and rough-surface parts (cross in Fig. 6) give younger apparent ages of 74–154 Ma. Except these, the rest 80 data (circle in Fig. 6), showing 1.72–17.83% $ThO_2$, 0.00–0.38% $UO_2$ and 0.019–0.141% PbO, yield an isochron of 172±5 Ma (MSWD=0.45) with an intercept value −0.0003±0.0012. The core age corresponds to the age for the sillimanite-garnet gneiss of the Gyeonggi Gneiss Complex in which the two-mica granite intruded. The older cores are xenocrysts derived from surrounding gneisses. They might survive from entire loss of Pb during the granite consolidation, since the closure temperature of Pb diffusion in monazite (650–700°C, Suzuki et al., 1994) is close to the solidus temperature of hydrous granitic magma at moderate pressures (Stern et al., 1975).

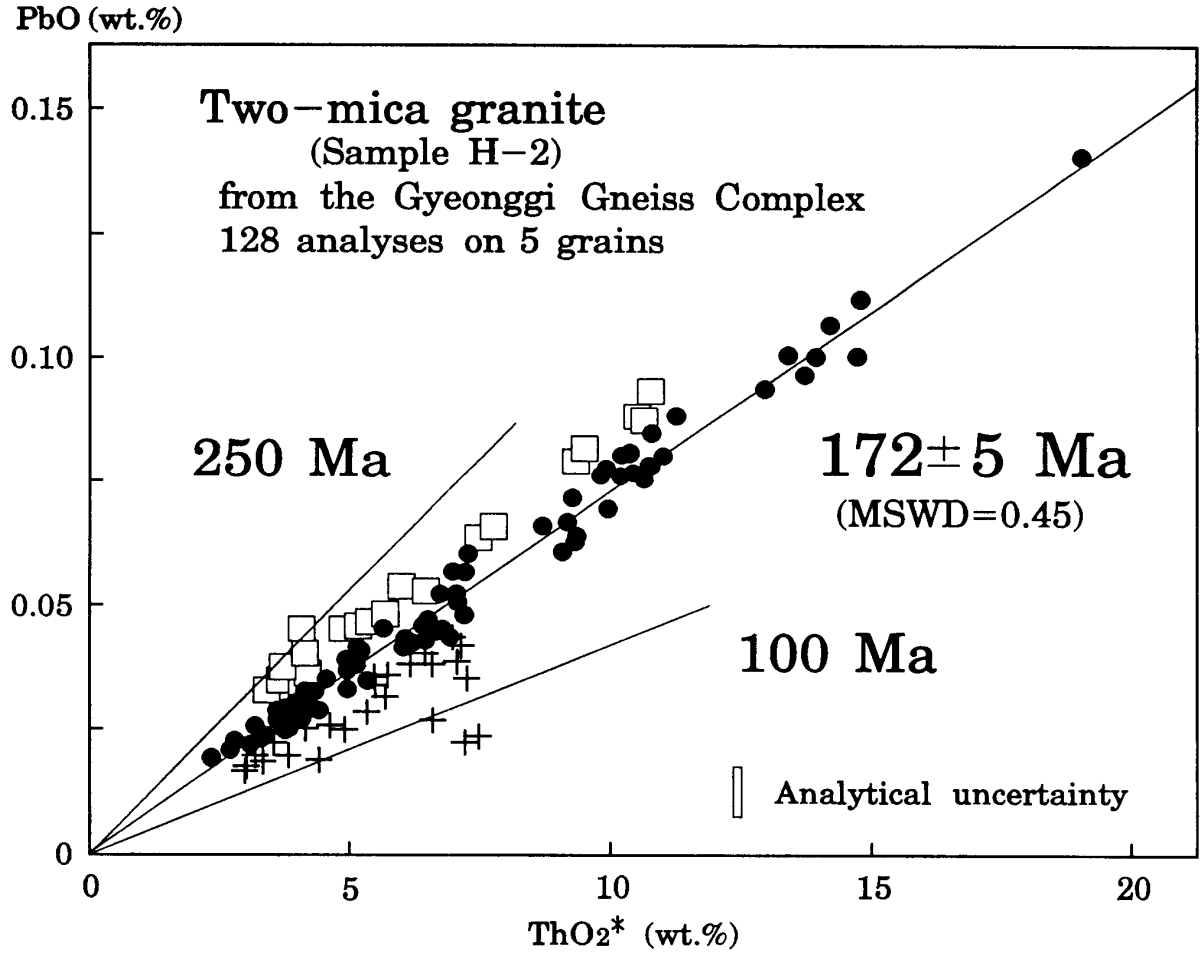


Fig. 6. Plots of PbO vs. $ThO_2$* of monazite grains from the two-mica granite (sample H-2) in the Gyeonggi Gneiss Complex. Circles represent data points used for age calculation. Data points for core and rim portions of individual grains are shown by squares and crosses, respectively. Explanation for errors is the same as Fig. 3.

K-Ar muscovite age of this two-mica granite is 151 ± 4 Ma (Park et al., 1997). The blocking temperature of muscovite (350 ± 50°C, Dodson and McClelland-Brown, 1985) is lower than that of monazite (650–700°C, Suzuki et al., 1994). Since most of the Jurassic Daebo Granites cooled slowly at middle crust level (Cho and Kwon, 1994) after the consolidation, the CHIME monazite and K-Ar muscovite ages are reasonably regarded as the time of emplacement and subsequent cooling of the two-mica granite.

## DISCUSSION

Monazite begins to form as metamorphic mineral at the lower amphibolite-facies condition (Smith and Barreiro, 1990). Thus, the CHIME monazite age of 255 ± 8 Ma for the kyanite-staurolite-garnet schist can be regarded as the time of the regional metamorphism for the early-middle Proterozoic Yeoncheon Group in the so-called Imjingang Fold Belt. The metamorphic age for the

Yeoncheon Group was also dated through the Sm-Nd and Rb-Sr mineral isochron methods (Cho et al., 1995). The Sm-Nd and Rb-Sr garnet-plagioclase-whole rock isochron ages of amphibolite from the Misan Formation are 231±30 Ma and 224±24 Ma, respectively. Although the ages are overlapped within error limits, the CHIME monazite age appears to be significantly older than the isotopic ages. Presumably, the CHIME monazite age represents the time for the first attainment of the lower amphibolite facies, and the Sm-Nd and Rb-Sr ages date the time of cooling related to uplift.

The sillimanite-garnet gneiss from the Gyeonggi Gneiss Complex gives CHIME monazite age of 245±3 Ma. As stated earlier, this gneiss sample contains monazite with ca. 1700 Ma core of detrital origin. Therefore, the sedimentation age of the gneiss protolith is post-middle Proterozoic. This clearly demonstrates that all of the Gyeonggi Gneiss Complex is not the Archean—early Proterozoic complex so far believed (Na and Kim, 1987; Ri and Ri, 1994; Chwae, et al., 1995). The post-middle Proterozoic sediment underwent the late Permian-early Triassic amphibolite-facies metamorphism and the Jurassic thermal event.

Despite the different geologic province and tectonic setting (Figs. 1, 2 and 3), CHIME monazite ages for the Yeoncheon Group and the Gyeonggi Gneiss Complex are nearly identical. This suggests that the late Permian—early Triassic regional metamorphism occurred not only in the Imjingang Fold Belt but also in some parts of the Gyeonggi Gneiss Complex. The late Permian—early Triassic regional metamorphism is also recognized from the central part of the Ogcheon Fold Belt in the Korean Peninsula (Adachi et al., 1996). Outside the Korean Peninsula, the late Permian—early Triassic regional metamorphism occurred in the Hida Terrane, Southwest Japan (Suzuki and Adachi, 1994), the Qinling-Dabie-Sulu Collisional Belt, China (Liu, 1993) and so on. Although many hypotheses on the tectonic correlation of China-Korea-Japan-Russia have been proposed (Adachi et al., 1996; Suzuki and Adachi, 1994; Cluzel, 1992; Ernst et al., 1994, Liu, 1993; Yin and Nie, 1993), details in terms of tectonics are still unclear.

It is noteworthy that the metamorphic rocks of the Yeoncheon Group and the Gyeonggi Gneiss Complex are particularly comparable in mineral assemblage as well as in age with the Unazuki Schist of the Barrovian type and the Hida Gneiss of the Buchan type in the Hida terrane of central Japan, respectively. The Yeoncheon Group and the Gyeonggi Gneiss Complex were extensively intruded by the Jurassic Daebo Granites including the 172±5 Ma two-mica granite, and the Unazuki Schist and the Hida Gneiss in central Japan were intruded by the ca. 175—190 Ma (Shibata and Nozawa, 1984; Khan et al., 1995) Funatsu Granite. The overall similarity in metamorphic age, mineral assemblage and plutonic age shows that both the Gyeonggi Massif in the Korean Peninsula and the Hida terrane in central Japan once shared a common geologic province.

## CONCLUDING REMARKS

On the basis of the preliminary CHIME geochronological study we can draw the following conclusions on the Gyeonggi Massif including the Yeoncheon Group.

(1) The CHIME monazite age for the kyanite-staurolite-garnet schist from the Yeoncheon Group is 255±8 Ma.

(2) The sillimanite-garnet gneiss from the central part of the Gyeonggi Gneiss Complex shows a CHIME monazite age of 245±3 Ma. This suggests that some parts of the Gyeonggi Gneiss Complex formed through the late Permian-early Triassic regional metamorphism.

(3) The ca. 250 Ma metamorphic ages revealed in the Gyeonggi Massif are equivalent to the age for the regional metamorphism in the central part of the Ogcheon Fold Belt in Korea, the Hida Terrane in Japan, and the Qinling-Dabie-Sulu Collisional Belt in China. Presumably, the ca. 250 Ma metamorphism and plutonism took place more widely in East Asia than has been thought.

(4) The ca. 1700 Ma core in a monazite grain from the sillimanite-garnet gneiss in the Gyeonggi Gneiss Complex constrains the sedimentation age of the gneiss protolith to be post-middle Proterozoic.

(5) The two-mica granite intruding the Gyeonggi Gneiss Complex yields a CHIME monazite age of 172±5 Ma.

## ACKNOWLEDGEMENTS

We thank Drs. S.J. Choi and K.H. Park at KIGAM for their discussion on the geologic setting and collecting samples, and Mr. S. Yogo of Nagoya University for his excellent technical assistance. One of the authors, D.L. Cho, would like to express his profound thanks to KIGAM and Department of Earth and Planetary Sciences, Nagoya University for providing an opportunity for research.

## REFERENCES

Adachi, M., Suzuki, K. and Chwae, U.C. (1996) CHIME age determination of metamorphic rocks in the Ockchon Belt, Korea. *Abstract of the 103rd Annual Meeting of the Geol. Soc. Japan*, 80.

Cho, D.L. and Kwon, S.T. (1994) Hornblende geobarometry of the Mesozoic granitoids in South Korea and the evolution of crustal thickness. *J. Geol. Soc. Korea*, **30**, 41–61.

Cho, M., Kwon, S.T., Ree, J.H. and Nakamura, E. (1995) High pressure amphibolite of the Imjingang belt in the Yeoncheon-Cheongok area. *J. Petrol. Soc. Korea*, **4**, 1–19.

Chwae, U.C., Choi, S.J., Park, K.H. and Kim, K.B. (1996) Explanatory text of the geological map of Cheolwon-Majeonri sheets (scale 1:50,000). Korea Inst. Geol. Mining and Materials, 1–31.

Chwae, U.C., Kim, K.B., Hong, S.H., Lee, B.J., Hwang, J.H., Park, K.H., Hwang, S.K., Choi, B.Y., Song, K.Y. and Jin, M.S. (Compilers) (1995) Geological map of Korea (scale 1:1,000,000). Korea Inst. Geol. Mining and Materials.

Cluzel, D. (1992) Ordovician bimodal magmatism in the Ogcheon belt (South Korea): Intracontinental rift related volcanic activity. *J. Southeast Asian Earth Sci.*, **7**. 195–209.

Cluzel, D., Lee, B.J. and Cadet, J.P. (1991) Indosinian dextral ductile fault system and synkinematic plutonism in the southwest of the Ogcheon Belt (South Korea). *Tectonophysics*, **10**, 131–152.

Dodson, M.H. and McClelland-Brown, E. (1985) Isotopic and paleomagnetic evidence for rates of cooling, uplift and erosion. *Geol. Soc. Mem.*, **10**, 315–325.

Ernst, W.G., Liou, J.G. and Harker, B.R. (1994) Petrotectonic significance of high- and ultrahigh-pressure metamorphic belts: Inferences for subduction zone history. *Int. Geol. Rev.*, **36**, 213–237.

Khan, I.H, Suzuki, K., Shibata, K. and Adachi, M. (1995) Late Permian CHIME ages of the Hida Gneiss and early Triassic age of the Mizunashi Granite in the Amo area of the Hida terrane, central Japan. *J. Earth Planet. Sci., Nagoya Univ.*, **42**, 31–43.

Lee, S.R. and Cho, M. (1994) Granulite in the Hwacheon-Yanggu area. *Abstract and Program, Geol. Sco. Korea*, 73.

Lee, D.S., Lee, H.Y., Nam, K.S. and Yang, S.Y. (1974) Explanatory text of the geological map of Chucheon sheet (scale 1:50,000). Geol. and Mineral Inst. Korea, 1–9.

Liu, X. (1993) High-P metamorphic belt in central China and its possible eastward extension to Korea. *J. Petrol. Soc. Korea*, **2**, 9–18.

Na, K.C. (1977) The geology and granitization of northeastern Gyeonggi Massif. *Res. Rev. Chungbuk Univ.*, **15**, 57–66.

Na, K.C. (1978) Regional metamorphism in the Gyeonggi Massif with comparative studies on the Yeoncheon and Ogcheon metamorphic belts (I), (on the general geology and petrography of Gyeonggi Massif). *J. Geol. Soc. Korea*, **14**, 195–211.

Na, K.C. and Kim, H.S. (1987) Precambrian Eonothem. In: *Geology of Korea* (ed. D.S. Lee). Geol. Soc. Korea (Kyohaksa Co., Seoul), 17–48.

Na, K.C. and Lee, D.J. (1973) Preliminary age study of the Gyeonggi metamorphic belt by the Rb-Sr whole rock method. *J. Geol. Soc. Korea*, **19**, 168–174.

Park, K.H., Lee, B.J., Cho, D.L. and Kim, J.B. (1977) Explanatory text of the geological map of Hwacheon Sheet (scale 1:50,000). Korea Inst. Geol. Mining and Materials (in press).

Ri, J.N. and Ri, J.C. (1990) Geological constitution of Korea. Industrial Publishing House, **6**, 216p.

Ri, J.N. and Ri, J.C. (Editors) (1994) Tectonic map of Korea (scale 1:1,000,000) and explanatory text. Central Geol. Survey, Pyongyang, 22p.

Shibata, K. and Nozawa, T. (1984) Isotopic ages of the Funatsu Granitic Rocks. *J. Japan. Assoc. Min. Pet. Econ. Geol.*, **79**, 289–298.

Smith, H.A. and Barreiro, B. (1990) Monazite U-Pb dating of staurolite grade metamorphism in pelitic schist. *Contrib. Mineral. Petrol.*, **105**, 602–615.

Stern, C.R., Hwang, W. and Wyllie, P.J. (1975) Basalt-andesite-rhyolite-$H_2O$: Crystallization intervals with excess $H_2O$ and $H_2O$ undersaturated liquidus surfaces to 35 kilobars, with implication for magma genesis. *Earth Planet. Sci. Lett.*, **28**, 189–196.

Suzuki, K. and Adachi, M. (1991a) Precambrian provenance and Silurian metamorphism of the Tsubonosawa paragneiss in the South Kitakami terrane, Northeast Japan, revealed by the chemical Th-U-total Pb isochron ages of monazite, zircon and xenotime. *Geochem. J.*, **25**, 357–376.

Suzuki, K. and Adachi, M. (1991b) The chemical Th-U-total Pb isochron ages of zircon and monazite form the Gray Granite of the Hida terrane, Japan. *J. Earth Sci., Nagoya Univ.*, **38**, 11–37.

Suzuki, K. and Adachi, M. (1994) Middle Precambrian detrital monazite and zircon from the Hida gneiss on Oki-Dogo Island, Japan: their origin and implications for the correlation of basement gneiss of Southwest Japan and Korea. *Tectonophysics*, **235**, 277–292.

Suzuki, K., Adachi, M. and Kajizuka, I. (1994) Electron microprobe observations of Pb diffusion in metamorphosed detrital monazites. *Earth Planet. Sci. Lett.*, **128**, 391–405.

Suzuki, K., Adachi, M. and Tanaka, T. (1991) Middle Precambrian provenance of Jurassic sandstone in the Mino terrane, central Japan: The Th-U-total Pb evidence from an electron microprobe monazite study. *Sediment. Geol.*, **75**, 141–147.

Yin, A. and Nie, S. (1993) An indentation model for the North and South China collision and the development of the Tan-Lu and Honam fault system, eastern Asia. *Tectonics*, **12**, 801–813.